福昕PDF编辑器

• 永久 • 轻巧 • 自由

升级会员

批量购买

永久使用
无限制使用次数

极速轻巧
超低资源占用，告别卡顿慢

自由编辑
享受Word一样的编辑自由

扫一扫，关注公众号

Journal of Colloid and Interface Science 581 (2021) 195–204

Contents lists available at ScienceDirect

Journal of Colloid and Interface Science

journal homepage: www.elsevier.com/locate/jcis

Heterogeneous activation of peroxymonosulfate by cobalt-doped MIL-53 (Al) for efficient tetracycline degradation in water: Coexistence of radical and non-radical reactions

Fang Liu [a,b,1], Jiao Cao [a,b,1], Zhaohui Yang [a,b,*], Weiping Xiong [a,b], Zhengyong Xu [c], Peipei Song [d], Meiying Jia [a,b], Saiwu Sun [a,b], Yanru Zhang [a,b], Xuexin Zhong [e]

[a] College of Environmental Science and Engineering, Hunan University, Changsha 410082, PR China
[b] Key Laboratory of Environmental Biology and Pollution Control (Hunan University), Ministry of Education, Changsha 410082, PR China
[c] Science and Technology Service Center of Hunan Province, Changsha 410128, PR China
[d] College of Resources and Environment, Key Laboratory of Agricultural Environment, Shandong Agricultural University, Tai'an 271000, PR China
[e] Hunan Xinheng Environmental Technology Co Ltd, Changsha 410005, PR China

GRAPHICAL ABSTRACT

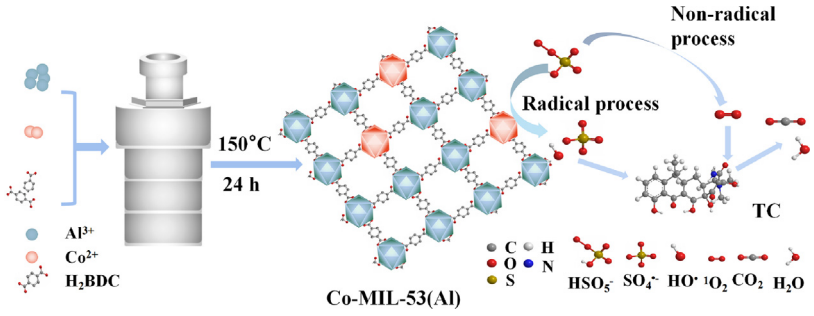

ARTICLE INFO

Article history:
Received 8 April 2020
Revised 19 July 2020
Accepted 20 July 2020
Available online 25 July 2020

Keywords:
Co-doped MIL-53(Al)
Heterogeneous system
Peroxymonosulfate
Tetracycline
Sulfate radicals
Singlet oxygen

ABSTRACT

Compared with the transition metal induced homogeneous catalytic system, the heterogeneous catalytic system based on transition metal-doped metal organic frameworks (MOFs) were stable for the efficient utilization of transition metal and avoiding the metal leaching. The aim of this work is to synthesize Co-doped MIL-53(Al) by one-step solvent thermal method and use it to activate peroxymonosulfate (PMS) to remove tetracycline (TC) in water. The successful synthesis of Co-MIL-53(Al) samples was demonstrated by XDR, SEM and FTIR characterizations. The 25% Co-MIL-53(Al)/PMS system showed the optimal TC removal effect compared to the PMS alone and MIL-53(Al)/PMS system. The catalytic performances of Co-MIL-53(Al)/PMS system in conditions of different pH, co-existing substances and water bodies were investigated. Quenching experiment and electron paramagnetic resonance (EPR) showed that the degradation mechanism by Co-MIL-53(Al) activation PMS was mainly attributed to sulfate radical ($SO_4^{\bullet-}$) and singlet oxygen ($^1O_2$) non-radical. The degradation intermediates of TC were also identified and the possible degradation pathways were proposed. Co-MIL-53(Al) showed good activity after four cycles. These findings demonstrated that Co-MIL-53(Al) can be a promising heterogeneous catalyst for activating PMS to degrade TC.

* Corresponding author at: College of Environmental Science and Engineering, Hunan University, Changsha, Hunan 410082, PR China.
E-mail address: yzh@hnu.edu.cn (Z. Yang).
[1] These authors contribute equally to this article.

https://doi.org/10.1016/j.jcis.2020.07.100
0021-9797/

1. Introduction

In recent decades, water pollution has been an urgent and non-negligible problem in the world [1,2]. As a new type of pollutants, antibiotics attract extensive attention. Antibiotics have been over-used in recent years, and the accumulation of antibiotics may lead to a significant increase of antibiotic resistance of microorganisms. And antibiotics may cause problems with target organisms such as endocrine disruption, chronic toxicity in the long term [3,4]. Tetracycline (TC) is one of the most widely used antibiotics with stable structure, and it is difficult to remove by traditional biological methods [5–7].

Advanced oxidation processes (AOPs) have a wide application prospect because of their fast degradation rate, high oxidation efficiency and effective degradation towards various pollutants in the environment [8,9]. Recently, AOPs based on sulfate radical ($SO_4^{\bullet-}$) receive increasing attention because of their effective degradation towards organic compounds. The $SO_4^{\bullet-}$ has a higher oxidative potentials (2.5–3.1 V vs 1.8–2.7 V of HO•), a longer half-life (30–40 μs vs 20 ns of HO•), and a wider range of pH (pH from 2 to 8) than the hydroxyl radical (HO•) that plays a major role in the Fenton reaction [10–12]. In general, peroxydisulfate (PDS) and peroxymonosulfate (PMS) are two sulfates that can be activated by catalysts to produce $SO_4^{\bullet-}$ [13]. The structures $^{-}O_3S—O—O—SO_3$ and O—O contained in PDS are symmetric and the O—O bond length of PDS is 1.322 Å. However, the HO-O-SO_3^- in the PMS is asymmetric and PMS contains longer superoxide O—O bond (I_{O-O} = 1.326 Å). These properties make PMS easier to be activated than PDS [14].

The transition metals activation of PMS receives a lot of attention because of its obvious advantages: low energy consumption and easy operation [15,16]. Transition metals can activate PMS mainly because of electron transfer. A transition metal at a low oxidation valence loses an electron to a higher valence state, and this electron is transferred to the HSO_5^- in PMS to form the $SO_4^{\bullet-}$, as shown in Eq. (1) [17]. At the same time, the formed $SO_4^{\bullet-}$ can also react with H_2O or OH^- to produce hydroxyl radical (HO·) that plays a role in the catalyst/PMS system according to Eq. (2) [18].

$$M^{n+} + HSO_5^- \rightarrow M^{(n+1)+} + SO_4^{\bullet-} + OH^- \quad (1)$$

$$SO_4^{\bullet-} + OH^-(H_2O) \rightarrow SO_4^{2-} + HO\cdot(+H^+) \quad (2)$$

Among the transition metals, iron (Fe) [19], manganese (Mn) [20], copper (Cu) [21] and cobalt (Co) were efficient to activate PMS. It was worth noting that some studies showed that Co^{2+} owned the best activation ability [11,22]. Homogeneous Co^{2+}/PMS system is effective to the contaminant purification, while the carcinogenic Co^{2+} brings threat to human health [23]. A series of researches showed that introducing Co into substrates to form heterogeneous catalysts could give play to the catalytic activity of Co. More importantly, the Co leaching threat was greatly reduced [24–26]. Therefore, in order to develop Co's ability to degrade pollutants without generation of secondary pollution, it is important to find a suitable carrier.

Metal organic frameworks (MOFs) are a kind of hybrid materials which are formed through connection between organic and inorganic units by strong bonds. In recent years, MOFs have arisen great interest in researchers for their superior properties: suitable pore structure, high specific surface area, large pore size [27–31]. MOFs doped with metal were extensively studied because of their great catalytic ability. The Cu-doped ZIF-8 synthesized by Nagarjun et al. showed better catalytic performance than pure ZIF-8. Moreover, the catalytic performance and morphology of Cu-doped ZIF-8 did not change significantly after two times of reusing [32]. Cao et al. added Co to UiO-66 for efficient catalytic removal of TC and the porosity of UiO-66 provided active sites for contact between the catalyst and TC molecules [33]. The MIL series are one of the most widely studied types of MOFs. Researchers carried out some adsorption and catalytic experiments about MIL-53(Al) and found that MIL-53(Al) was of a kind of strong thermal and chemical stability in the MIL series. Therefore, it is feasible to select MIL-53(Al) for catalytic research.

Therefore, Co-MIL-53(Al) series with different Co contents were synthesized by one-step solvent-thermal method and the morphology, structure, porosity, chemical property were characterized. What's more, the removal efficiencies of TC by Co-MIL-53(Al)/PMS system under different PMS dosage, pH values, co-existing ions and actual wastewater were studied. For testing the stability of the catalyst, cyclic experiments were carried out. Quenching experiment and EPR test were conducted to explore the degradation mechanism. This study provided a new idea about the synthesis of transition metal doped catalysts in actual wastewater treatment.

2. Experimental

2.1. Materials

Aluminium chloride hexahydrate ($AlCl_3{\cdot}6H_2O$, ≥99.9%), Cobalt chloride hexahydrate ($CoCl_2{\cdot}6H_2O$, ≥99.9%), N, *N*-dimethylformamide (DMF, ≥99.5%), 1,4-benzendicarboxylic acid (H_2BDC, ≥99.0%), anhydrous ethanol (≥99.9%), methanol (≥99.5%), tertiary butanol (TBA, ≥99.9%), L-histidine (≥98.0%), humic acid (HA, ≥99.0%), sodium nitrate ($NaNO_3$, ≥99.0%), sodium chloride (NaCl, ≥99.0%) and sodium carbonate (Na_2CO_3, ≥99.0%) were provided by Sinopharm Chemical Reagent Co.,Ltd. Tetracycline (TC, ≥99.0%) and potassium peroxymonosulfate (PMS, 42.0%–47.0% $KHSO_5$ basis) were acquired from Shanghai Rhawn Technology Development Co. Ltd. All solutions in this study were prepared by deionized water (resistivity = 18.25 MΩ·cm, 25 °C) purified by Milli-Q system.

2.2. Syntheses

Preparation of MIL-53(Al): MIL-53(Al) was synthesized by mixed solvent thermal way with some modifications referring to the published literature [34]. 0.734 g $AlCl_3{\cdot}6H_2O$ was added to 11.25 mL deionized water and stirred to make solution 1. 0.77 g H_2BDC was dissolved in 33.75 mL DMF to form solution 2. Then the mixture of solution 1 and solution 2 was stirred for 1 h under room temperature, transferred into the 100 mL Teflon-lined steel reactor and put in an oven statically for 1 day under the condition of 150 °C. After the solution's temperature in the reactor decreased to room temperature, it was centrifuged and washed three times using DMF and anhydrous ethanol respectively to get the white product, MIL-53(Al). The obtained white product was placed in a vacuum drying oven and dried at 60 °C overnight.

Preparation of Co-MIL-53(Al): To get a series of cobalt-doped MIL-53(Al) (X Co-MIL-53(Al), X = 10%, 15%, 20%, 25% which represented the molar ratio of Co to Al), various amount of $CoCl_2{\cdot}6H_2O$ was added into solution 1 to get solution 3. Then solution 3 and 2 were mixed quickly. The following procedures were the same as synthesizing MIL-53(Al).

2.3. Instrumentation and characterization

X-ray diffraction (XRD, Bruker D8 Advance powder X-ray Cu Ka radiation diffractometer, wavelength is 0.15406 nm), Field emission scanning electron microscopy (FE-SEM, Zeiss Sigma HD), Fourier-transform infrared spectroscopy (FTIR, Bruker Vertex 70), static volumetric adsorption system (QUADRASORB SI), X-ray pho-

toelectron spectroscopy (XPS, EscaLab Xi +) and inductively coupled plasma mass spectrometry (ICP-MS, Aglient 7800).

2.4. Degradation experiments

The catalytic oxidation experiment was carried out in 250 mL beakers containing 100 mL TC solution at a concentration of 30 mg L^{-1}. The 20 mg sample was dispersed into TC solution for adsorption, and the time point of adsorption equilibrium was reached after 1 h. In general, this act is to avoid effect of the TC adsorption by catalyst on the evaluation of actual catalytic performance. Then 30 mg PMS was added to start catalytic degradation. In particular, in the influence experiment of PMS addition amount, the amounts of PMS were 10, 20, 30 and 40 mg. The degradation process lasted 1 h under magnetic stirring. At some regular time, sample solution was collected and UV–Vis spectrophotometer (Shimadzu, Japan) was used to measure the TC concentration at 357 nm.

3. Results and discussion

3.1. Structure characterization

The XRD patterns of MIL-53(Al) and MIL-53(Al) doped with different amounts of Co were shown in Fig. 1. The crystallinity information about as-prepared samples could be obtained. The XRD pattern of the sample MIL-53 (Al) was consistent with that reported by other researcher [35]. This suggested that MIL-53 (Al) was synthesized successfully in this experiment. As could be seen from the XRD pattern, the diffraction peak (1 1 0) was shown at 2θ = 9.2°, and the diffraction peak (2 1 1) and (2 2 0) combined to form one peak (2θ = 18.2°) [34]. After Co doping into MIL-53(Al), the characteristic diffraction peak basically did not change, indicating that the Co doping did not change the crystalline shape of MIL-53(Al) [33]. But the peak strength of Co-MIL-53 (Al) was lower than that of pure MIL-53 (Al), possibly because of the negative effect of Co doping on the crystallization properties of the material. It was worth noting that there was no peak of Co species and possibly because the actual doping content of Co into MIL-53(Al) was very low [33].

SEM analysis of Fig. 2(a, b) and Fig. 2(c, d) showed the morphological features of the synthesized samples. MIL-53(Al) and 25% Co-MIL-53(Al) exhibited the similar morphology, both of which were cubic long strips, showing that Co doping did not change the structure of MIL-53 (Al). This conclusion also provided evidence to support the XRD results. After doping Co, the average diameter of sample was shortened by 9 nm, from 84 nm to 75 nm.

Fig. 3(a) provided such information that the FTIR spectra of MIL-53(Al), 10% Co-MIL-53(Al), 15% Co-MIL-53(Al), 20% Co-MIL-53(Al) and 25% Co-MIL-53(Al) were consistent. This phenomenon proved that Co doping did not change the functional groups of the samples. This conclusion was consistent with the conclusions obtained from XRD patterns and SEM images. There was a peak at 778 cm^{-1}, possibly caused by the bending vibration of C—H in the benzene ring [34]. The peaks at 1440 cm^{-1} and 1582 cm^{-1} were attributed to the C=C double bond vibration in the benzene ring [34]. The symmetric and asymmetric stretching of the –COO in carboxyl group of organic ligand H_2BDC contributed the peaks of 1402 cm^{-1} and 1607 cm^{-1} [36]. There might be some adsorbed water on the surface of samples, so the stretching vibration of –OH in the water caused the peak at 3449 cm^{-1} [37].

To further explore the BET surface area, pore diameter and pore volume of MIL-53(Al) and 25% Co-MIL-53(Al), N_2 adsorption and desorption experiment was carried out, and the obtained conclusions were demonstrated in Fig. 3(b) and Table. 1. The N_2 adsorption and desorption isotherms of the synthesized samples were all type IV hysteretic loops, indicating that the samples contained abundant micropores. The information could be obtained from the pore diameter distribution diagram inserted in Fig. 3(b) that the pore diameter mainly concentrated at 0–5 nm. The BET surface area of 25% Co-MIL-53(Al) was 905.02 $m^2\ g^{-1}$, which was lower than that of pure MIL-53(Al) (1127.10 $m^2\ g^{-1}$). The values of BET surface area of both MIL-53 (Al) and 25% Co-MIL-53 (Al) were smaller than that in the literature [38]. One possible reason was the samples were filled with H_2BDC remained. In addition, the FTIR spectrum showed the presence of adsorbed water in the samples and the water molecules contained in the samples also had a negative effect on BET surface area. The pore diameter and volume of the 25% Co-MIL-53(Al) did not change significantly compared to that of pure MIL-53(Al).

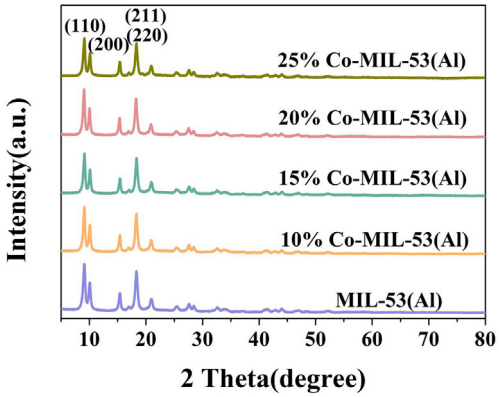

Fig. 1. XRD patterns of MIL-53(Al), (10%, 15%, 20%, 25%) Co-MIL-53(Al).

For clearly characterizing the chemical composition and valence of synthesized 25% Co-MIL-53(Al), XPS analysis was performed. It could be seen from survey spectrum in Fig. 4(a-d) that there were C, O and Al elements in 25% Co-MIL-53(Al). Since the doping amount of Co was very low, there was no obvious peak of Co element (Fig. 4(e)). According to the result of ICP-MS analysis, in the sample of 25% Co-MIL-53(Al), the actual amount of Co doped into MIL-53(Al) was only 1.3 wt%. These two outcomes verified the successful doping of Co with low content.

3.2. Catalytic performances

Before adding PMS, TC was adsorbed by samples. And after adding PMS, the degradation process of TC was studied. When discussing the degradation rate of TC, the time point of adding PMS was set to be t = 0. The degradation reaction lasted for 60 min. Pseudo-first order kinetics based on Langmuir–Hinshelwood model (Eq. (3)) was used to fit the TC degradation curves. The pseudo-first-order rate constant, k_{obs}, was obtained by linear regression of Eq. (4), which is derived from Eq. (3) when t = 0, C = C_0:

$$-dC/dt = k_{obs}C$$

$$\ln(C_t/C_0) = -k_{obs}t$$

where C_0 and C_t are the TC concentration when adding PMS and the concentration at degradation time t, respectively.

3.2.1. Effect of Co doping content

The catalytic performance and corresponding kinetic behavior based on pseudo-first-order model of Co-MIL-53(Al)/PMS system for TC degradation were studied. The effect of Co doping content was studied. As shown in Fig. 5(a), TC amount dropped by 26.9%

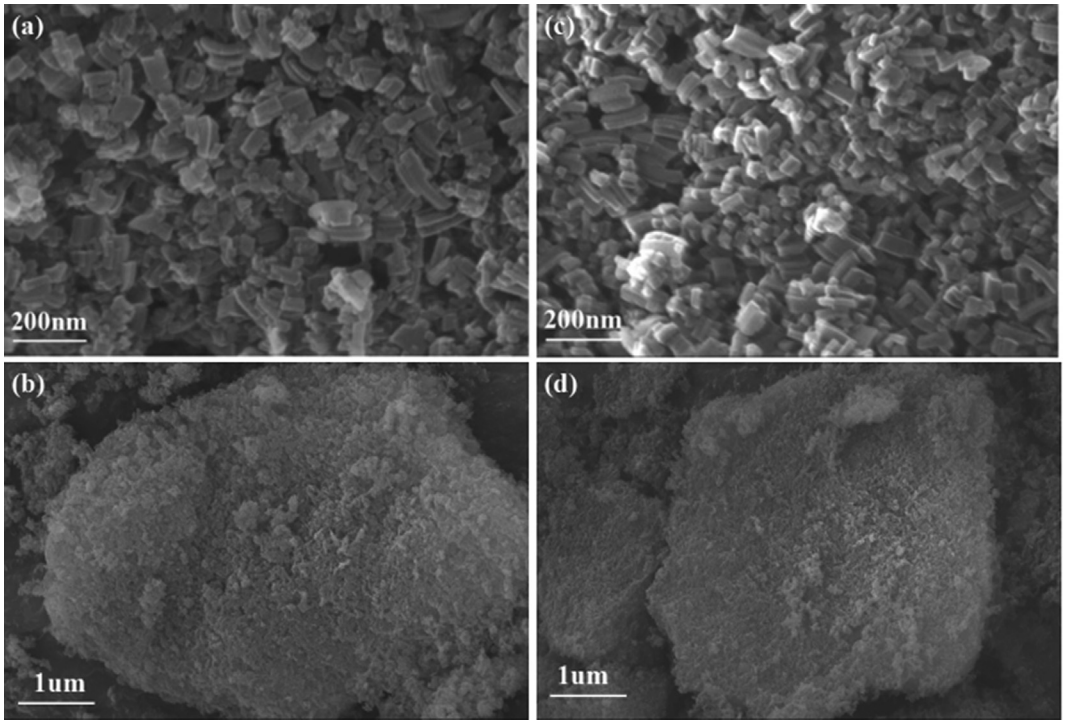

Fig. 2. SEM images of MIL-53(Al) (a, b) and 25% Co-MIL-53(Al) (c, d).

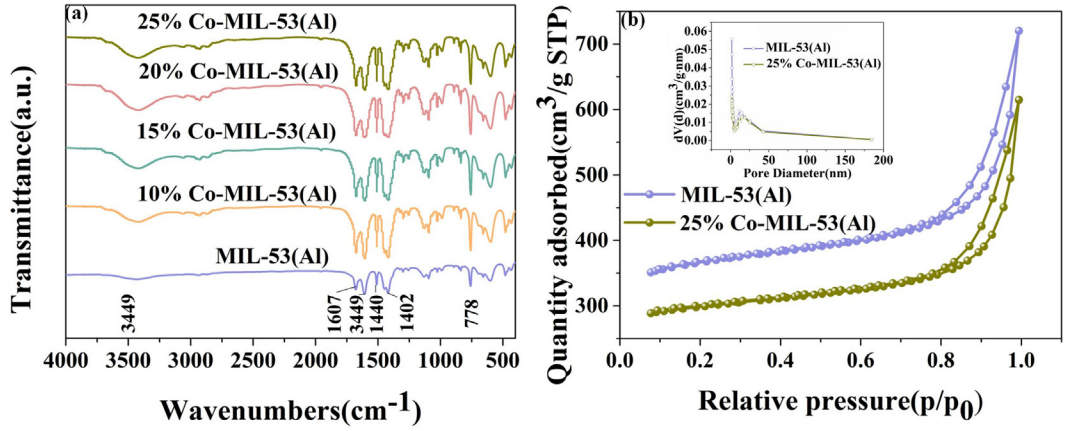

Fig. 3. FTIR spectra of MIL-53(Al) and (10%, 15%, 20%, 25%) Co-MIL-53(Al) (a) and N_2 adsorption/desorption isotherms (Inserted figure was the pore diameter distribution) of MIL-53(Al) and 25% Co-MIL-53(Al) (b).

Table 1
BET Surface area, pore diameter, pore volume of MIL-53(Al) and 25% Co-MIL-53(Al).

Samples	BET surface area[a] ($m^2\ g^{-1}$)	Pore diameter[b] (nm)	Pore volume[c] ($m^3\ g^{-1}$)
MIL-53(Al)	1112.71	1.63	0.64
25% Co-MIL-53(Al)	905.02	1.64	0.56

[a.]Measured using N_2 adsorption with the Brunauer-Emmett-Teller (BET) method.
[b.] Calculated by the desorption data using Barrett-Joyner-Halenda (BJH) method.
[c.]Total pore volume determined at P/P_0 = 0.99.

in the presence of PMS alone and the removal efficiency of TC was about 66.0% in MIL-53(Al)/PMS system. According to the test results of ICP-MS, the values of actual content of cobalt were 0.55 wt%, 0.79 wt%, 1.03 wt%1, .3 wt% in 10% Co-MIL-53 (Al), 15% Co-MIL-53 (Al), 20% Co-MIL-53 (Al) and 25% Co-MIL-53 (Al). Compared with pure MIL-53(Al), MIL-53(Al) doped with different Co contents greatly improved the removal efficiency. The systems of 10% Co-MIL-53(Al)/PMS, 15% Co-MIL-53(Al)/PMS, 20% Co-MIL-53(Al)/PMS and 25% Co-MIL-53(Al)/PMS reduced the TC concentration by 83.0%, 89.8%, 92.3% and 94.0% and the k_{obs} increased from 0.01708 min^{-1} to 0.03098 min^{-1} with the increasing Co content. This might be because the higher the cobalt content, the more efficient it was to activate PMS.

In the degradation curve of TC in 25% Co-MIL-53 (Al)/PMS system, the removal of TC was caused by the adsorption of catalyst and degradation of active substances produced by PMS activation by catalyst. The adsorption of TC by catalyst might be attributed to its large specific surface area [39]. Moreover, the catalyst provided a site for the activation of PMS and made it easier for the $SO_4^{\cdot-}$, $HO\cdot$ radicals and $^1O_2$ non-radical to interact with adsorbed TC molecules.

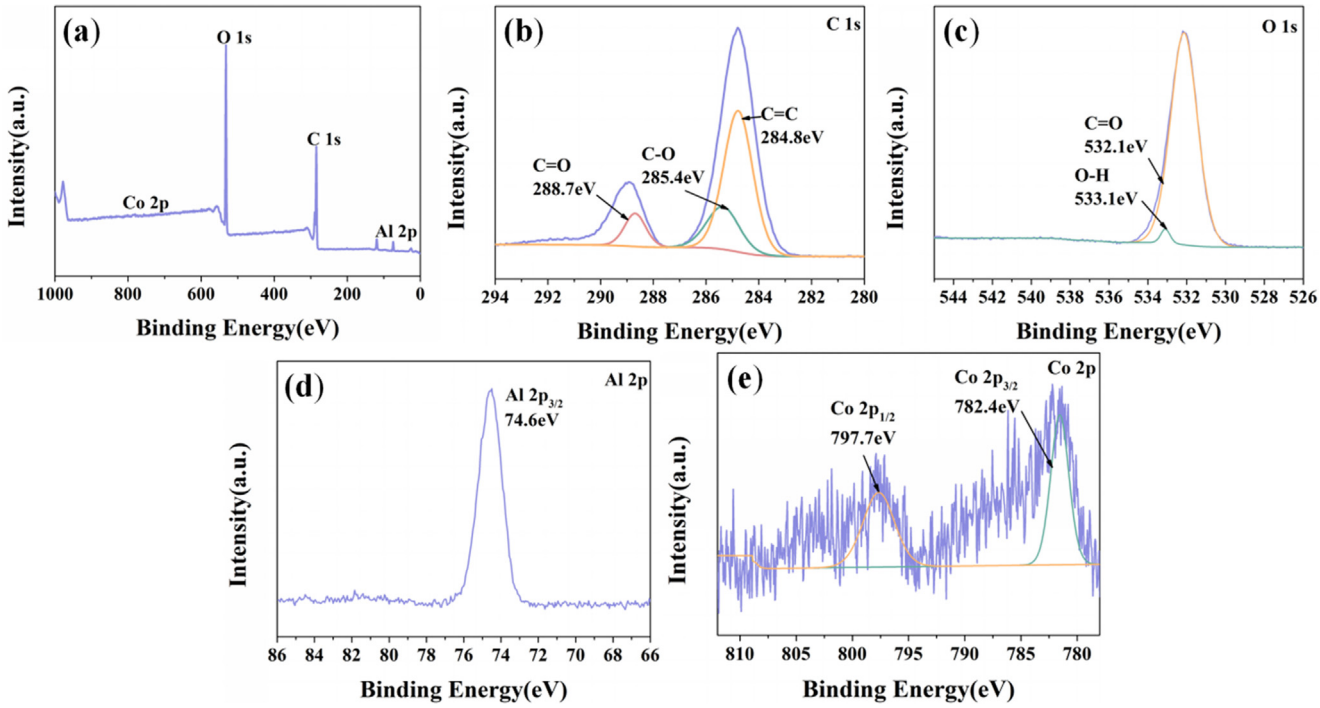

Fig. 4. XPS survey spectrum (a), C 1 s scanning spectrum (b), O 1 s scanning spectrum (c), Al 2p scanning spectrum (d), Co 2p scanning spectrum (e) of 25% Co-MIL-53(Al).

3.2.2. Effect of PMS dosage

Effect of PMS dosage on degradation effect was investigated. When the amount of PMS varied from 10 mg to 30 mg, the removal efficiency of TC improved continuously and the k_{obs} also increased. The increases in removal efficiency and speed were mainly because of the more active substances produced (Fig. 5(c)) [40]. However, when the amount of PMS increased to 40 mg, the removal efficiency and k_{obs} of TC decreased, which might be attributed to the self-quenching effect of excessive free radicals [41].

3.2.3. Effect of original pH value

The degradation of TC in the catalyst/PMS system might be affected by the original pH value of the solution according to previous report [18]. As was shown in Fig. 5(e), the 25% Co-MIL-53 (Al)/PMS system displayed high removal efficiency towards TC in a wide pH range of 3–11. In acidic solution (pH = 3, 5), the catalyst surface had a positive charge under the action of H^+ to better attract PMS [42]. When it came to alkaline condition, OH^- promoted the generation of $SO_4^{\cdot-}$ and HO·, two free radicals, to degrade TC by PMS [18].

3.2.4. Effect of co-existing ions and water bodies

To further explore the practical application of 25% Co-MIL-53 (Al), experiments were conducted in the environment of co-existing ions and different water bodies. As was shown in Fig. S2 (a, b) and Fig. S3(a, b), in the solution containing different concentrations of humic acid and NO_3^-, the removal efficiency and the k_{obs} were almost unchanged, which indicated the TC degradation process by 25% Co-MIL-53(Al)/PMS system was largely unaffected by humic acid and NO_3^-. Fig. S4(a, b) showed that when the concentration of Cl^- increased from 0 mM to 10 mM, there was a decrease of 7.7% in the degradation efficiency and the k_{obs} also went down from 0.03098 min^{-1} to 0.02354 min^{-1}. The possible reason was that Cl^- reacted with $SO_4^{\cdot-}$ and HO· to reduce the concentration of the two free radicals according to Eqs. (5, 6) [43] and Eqs. (7, 8, 6) [44]. The degradation of TC was to some extent negatively affected by the presence of CO_3^{2-} as shown in the removal efficiency diagram and the inserted degradation rate constant diagram of Fig. S6(a, b). The reason maybe that CO_3^{2-} scavenged part of $SO_4^{\cdot-}$ and HO· and less reactive species generated as Eqs. (9, 10) showed [45]. Obviously, in Fig. S7(a, b), although the removal efficiency and k_{obs} were slightly reduced compared to the ultrapure water environment, 25% Co-MIL-53(Al)/PMS system still displayed excellent removal efficiency in tap water, river water and pharmaceutical wastewater (the quality parameters of water bodies were given in Table. S1 in Supplementary Material). Inorganic ion impurities in tap water, Xiang river water and other co-existing organic compounds in pharmaceutical wastewater all affected the degradation process of TC. The above results showed that 25% Co-MIL-53(Al)/PMS system had the possibility to be applied to actual wastewater treatment.

$$SO_4^{\cdot-} + Cl^- \rightarrow Cl\cdot + SO_4^{2-}$$

$$Cl\cdot + Cl^- \rightarrow Cl_2^{\cdot-}$$

$$Cl^- + HO\cdot \rightarrow ClOH^-$$

$$ClOH^- + H^+ \rightarrow H_2O + Cl\cdot$$

$$CO_3^{2-} + SO_4^{\cdot-} \rightarrow SO_4^{2-} + CO_3^{\cdot-}$$

$$CO_3^{2-} + HO\cdot \rightarrow OH^- + CO_3^{\cdot-}$$

3.3. Comparison of other catalytic systems and stability test

In addition, compared with catalyst/PMS systems for TC removal in previous literatures [46–49], the catalytic system in this study had the advantages of low consumption of PMS and high removal efficiency (Table S2). Cyclic experiments were conducted to study the stability of 25% Co-MIL-53(Al) synthesized. The relevant results were shown in Fig. 6. After four cycles, the

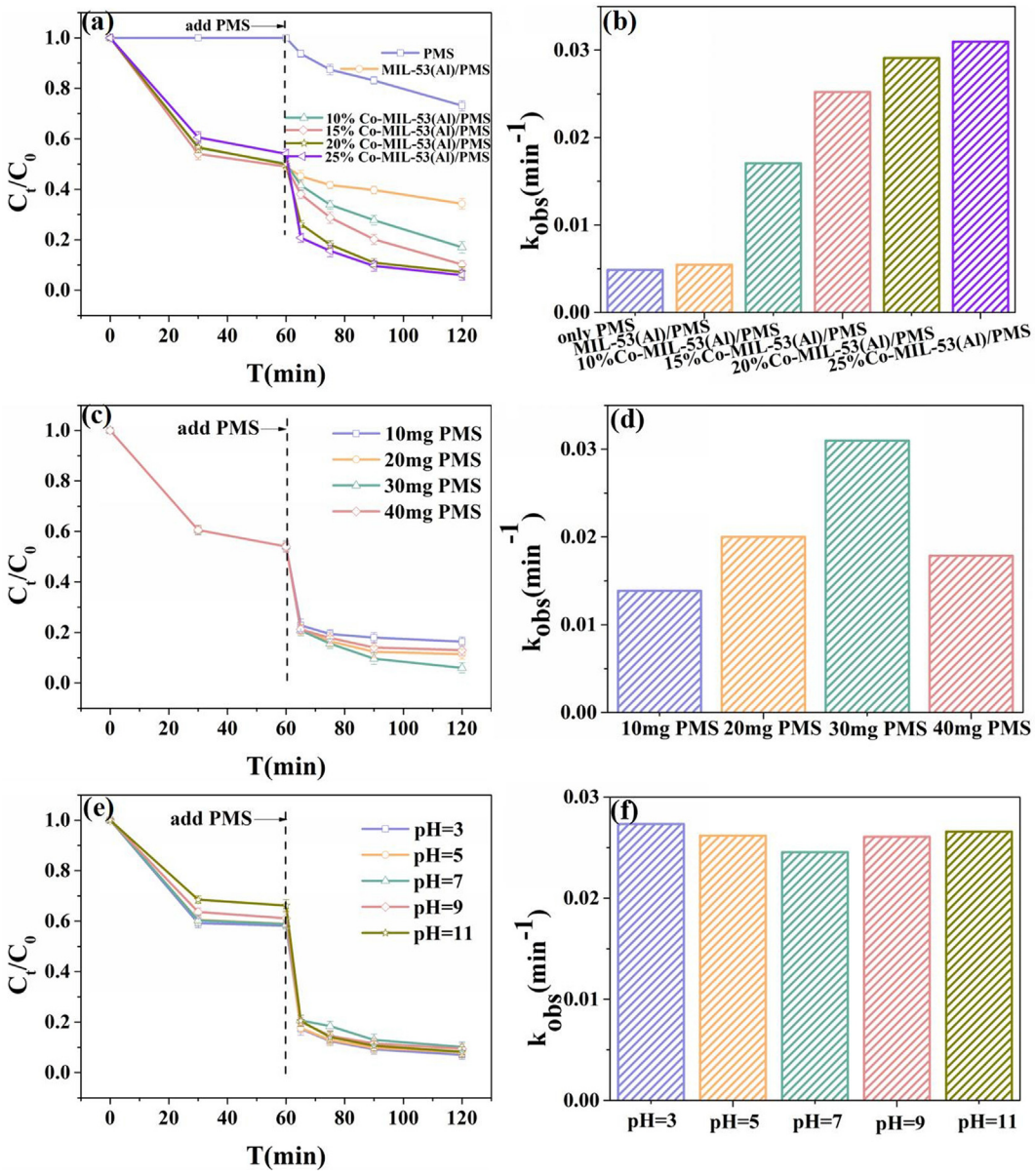

Fig. 5. TC degradation under different catalysts (a) (Experimental conditions: [catalyst] = 0.2 g L^{-1}; [PMS] = 0.3 g L^{-1}; [TC] = 30 mg L^{-1}; [Temp] = 298 K), different dosage of PMS (c) (Experimental conditions: [25% Co-MIL-53(Al)] = 0.2 g L^{-1}; [TC] = 30 mg L^{-1}; [Temp] = 298 K), different initial solution pH (e) (Experimental conditions: [25% Co-MIL-53 (Al)] = 0.2 g L^{-1}; [PMS] = 0.3 g L^{-1}; [TC] = 30 mg L^{-1}; [Temp] = 298 K). Kinetic constant based on the pseudo-first-order model (b, d, f).

removal efficiency of TC and the degradation rate constant both decreased. The Co contents of 25% Co-MIL-53(Al) before and after cycling were analyzed by ICP-MS. The initial Co content of 25% Co-MIL-53(Al) was 1.3 wt% and after four cycles, the amount of Co in the collected sample fell to 1.0 wt%. Co might be leached out during catalytic experiments and in the recycle of catalyst, which led to the decrease of Co content and further contributed to the deterioration of catalytic effect. In addition, TC molecules and other impurities might exist in 25% Co-MIl-53(Al), which were harmful to catalytic effect. Despite this, after four cycles, the removal efficiency of TC in 25% Co-MIL-53(Al)/PMS system maintained a high level (80%). The FTIR spectra (Fig. 6(c)) between 25% Co-MIL-53(Al) used for the fourth time and the pristine 25% Co-MIL-53(Al) were consistent. The consistency indicated that the catalyst was stable. Results above all also illustrated the great potential of Co-MIL-53(Al)/PMS systems in wastewater treatment.

3.4. Possible active substances

As reported in the literature, advanced oxidation processes (AOPs) based on PMS were mainly performed by reactive oxygen species (ROS) of sulfate radicals ($SO_4^{\bullet-}$), hydroxyl radicals ($HO^{\bullet}$) and singlet oxygen ($^1O_2$) [12,50,51]. In order to identify radical and non-radical reactions of TC degradation by 25% Co-MIL-53 (Al)/PMS system, quenching experiments were carried out. Hydroxyl radicals ($HO^{\bullet}$) and singlet oxygen ($^1O_2$) were trapped by tertiary butanol (TBA) and L-histidine, respectively. In addition, methanol (MeOH) was selected to capture both hydroxyl radicals ($HO^{\bullet}$) and sulfate radicals ($SO_4^{\bullet-}$) [15]. According to the inhibitory effect of degradation, the effects of two free radicals and one non-free radical could be clarified. The results of Fig. 7(a) showed that both TBA and MeOH inhibited the degradation of TC while the magnitude of the effect was varied. TBA reduced the removal efficiency of TC slightly, from 94% to 90%, and the k_{obs} only

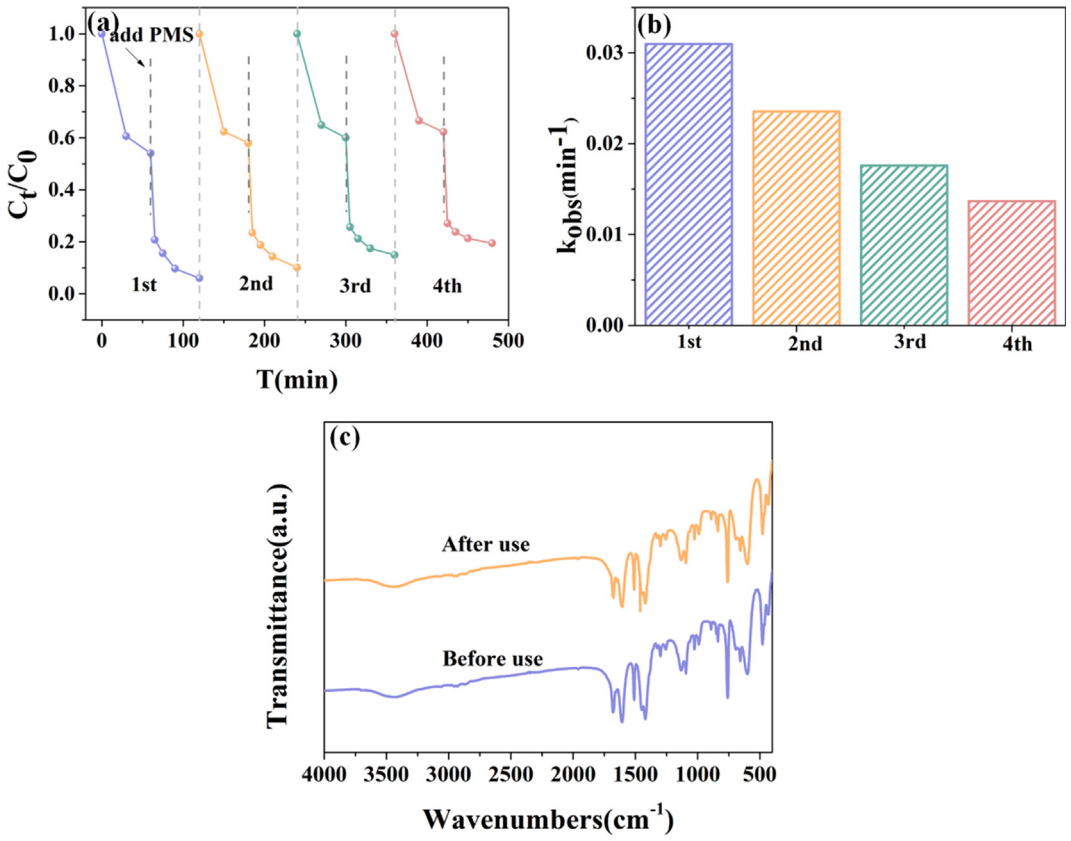

Fig. 6. Cycling tests of 25% Co-MIL-53(Al)/PMS system of TC degradation (a), kinetic constant based on the pseudo-first-order model (b) and FTIR spectra of 25% Co-MIL-53 (Al) before and after cycling (c). Experimental conditions: [25% Co-MIL-53(Al)] = 0.2 g L^{-1}; [PMS] = 0.3 g L^{-1}; [TC] = 30 mg L^{-1}; [Temp] = 298 K.

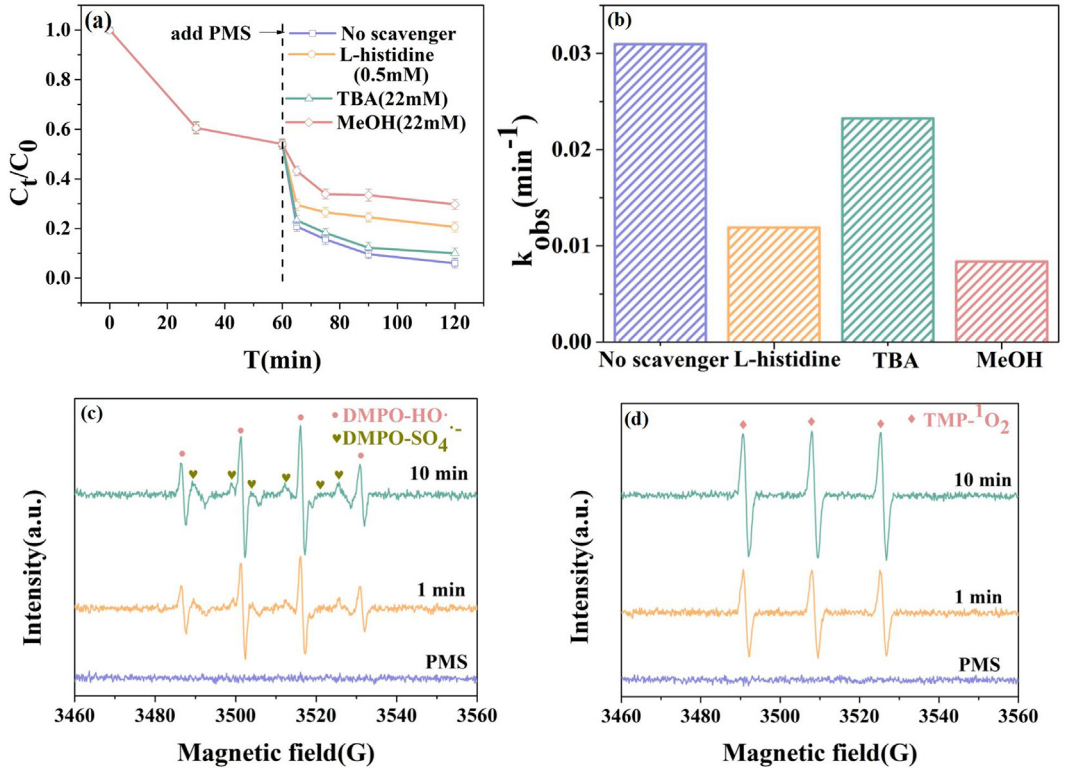

Fig. 7. TC degradation under different scavengers (a), kinetic constant based on the pseudo-first-order model (b); EPR spectra of 25% Co-MIL-53(Al)/PMS system in aqueous dispersion by spin trapping with DMPO (c) and TMP (d) at different time intervals. Experimental conditions: [25% Co-MIL-53(Al)] = 0.2 g L^{-1}; [PMS] = 0.3 g L^{-1}; [TC] = 30 mg L^{-1}; [Temp] = 298 K.

decreased by 0.00772 min^{-1}. However, the addition of MeOH made the removal efficiency decrease to 71%, especially the k_{obs} decrease dramatically from 0.03098 min^{-1} to 0.00836 min^{-1}. MeOH strongly inhibited the efficiency of TC degradation. The inhibition of TBA and MeOH indicated that the free radicals HO• and $SO_4^{\bullet-}$ were involved in the catalytic degradation of TC in 25% Co-MIL-53(Al)/PMS and $SO_4^{\bullet-}$ was dominant compared with HO•. When adding L-histidine (5 mM), the removal efficiency decreased from 94% to 80% and k_{obs} was reduced by 0.01907 min^{-1}. The negative effect of L-histidine indicated that non-radical $^1O_2$ played an important part in the degradation process. The conclusion of quenching experiments showed that $SO_4^{\bullet-}$ and $^1O_2$ were the main active substances.

To further confirm the results of quenching experiments, electron paramagnetic resonance (EPR) was applied. It was obvious from Fig. 7(c) that the characteristic signals of DMPO-$SO_4^{\bullet-}$ and DMPO-HO• were detected after the addition of 5, 5-dimethyl pyrroline oxide (DMPO). At 1 min and 10 min, there were obvious two characteristic signals of $SO_4^{\bullet-}$ and HO•, which indicated that 25% Co-MIL-53(Al) could indeed activate PMS to generate these two free radicals. For comparison, there were only weak signals in the PMS solution. The presence of $^1O_2$ was verified in the same way as the radicals, except that the additive was replaced by 2, 2, 6, 6-tetramethyl-4-piperidinol (TMP). Fig. 7(d) showed the appearance of TMP-$^1O_2$ signal, confirming the conclusion that $^1O_2$ was involved in the quenching experiment. The results of the above quenching experiments and EPR characterization brought the following information: $SO_4^{\bullet-}$ and $^1O_2$ were the main active components in the TC degradation process by 25% Co-MIL-53(Al)/PMS system.

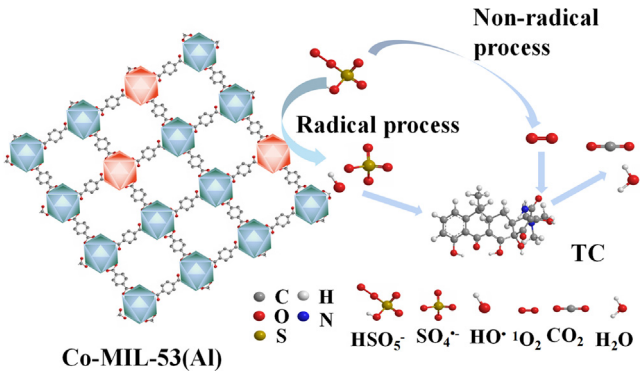

Fig. 8. The possible reaction mechanism of TC degradation in Co-MIL-53(Al)/PMS system.

3.5. Possible degradation mechanism

In the catalytic degradation process of TC by the 25% Co-MIL-53 (Al)/PMS system, the porosity of MIL-53(Al) was the attachment point of Co for PMS activation and also provided good active sites for contact between TC molecules and active substances. According to the above experimental results and the research conclusions reported in previous literatures [15,50], two different ideas of catalytic mechanism could be proposed. The first was the traditional process of metal ions activating PMS to generate radical species. As could be seen from the scanning spectra of Co 2p in Fig. 4(e), in the synthesized 25% Co-MIL-53(Al), Co element showed +2 and +3 valences, but mainly existed in the form of Co^{2+}. Co^{2+} catalyzed HSO_5^- components in PMS to generate $SO_4^{\bullet-}$ and OH^-, while Co^{2+} lost an electron and was oxidized to Co^{3+} (Eq. (11)). In addition, as shown in Eq. (12), Co^{3+} could also be reduced to Co^{2+}, and $SO_5^{\bullet-}$ and H^+ could be generated at the same time, which also ensured the continuous catalytic reaction [52]. The formed $SO_4^{\bullet-}$ might further react with OH^- to generate HO• (Eq. (13)) [18]. The second was a non-radical oxidation process. $SO_5^{\bullet-}$ radicals in PMS could react in pairs to produce $S_2O_8^{2-}$ and $^1O_2$ (Eq. (14)) [52]. SO_5^{2-} and HSO_5^- reacted to form $^1O_2$ (Eq. (15)). Eventually, the resulting $SO_4^{\bullet-}$ radicals and $^1O_2$ non-radicals degrade TC into H_2O and CO_2. The possible reaction mechanism of TC degradation by Co-MIL-53(Al)/PMS system were showed in Fig. 8.

$$Co^{2+} + HSO_5^- \rightarrow SO_4^{\bullet-} + Co^{3+} + OH^-$$

$$Co^{3+} + HSO_5^- \rightarrow SO_5^{\bullet-} + Co^{2+} + H^+$$

$$SO_4^{\bullet-} + OH^- \rightarrow SO_4^{2-} + HO\cdot$$

$$SO_5^{\bullet-} + SO_5^{\bullet-} \rightarrow S_2O_8^{2-} + {}^1O_2$$

$$SO_5^{2-} + HSO_5^- \rightarrow HSO_4^{2-} + {}^1O_2$$

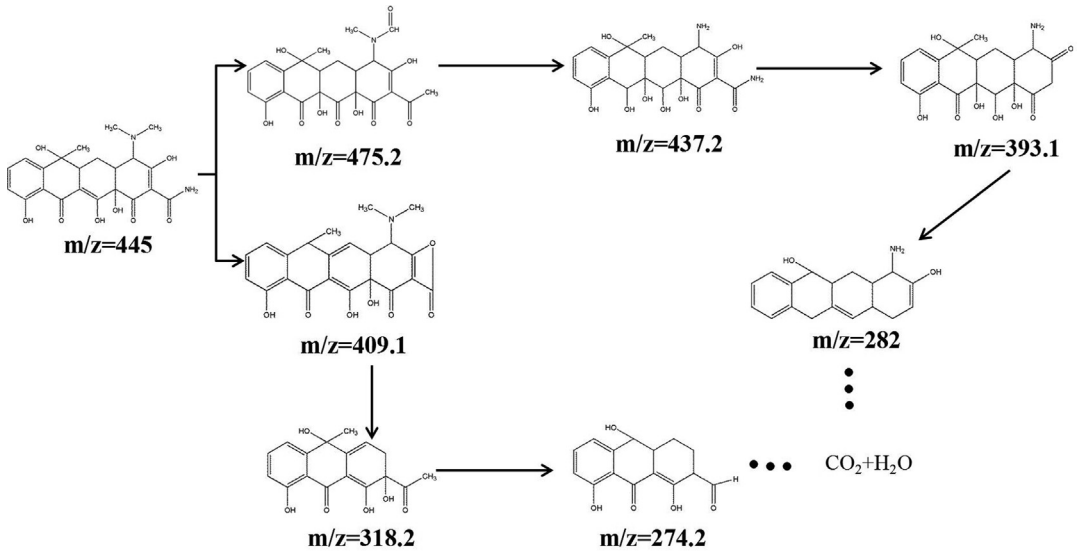

Fig. 9. Proposed pathways for the oxidative degradation of TC under 25% Co-MIL-53(Al)/PMS system.

3.6. TC degradation pathway

During the TC degradation, the intermediate products were detected by LC-MS (the analysis method was shown in Supplementary Material). The detected intermediates and their possible molecular structures including m/z = 274.2, m/z = 282, m/z = 318.2, m/z = 393.1, m/z = 409.1, m/z = 437.2, m/z = 445 and m/z = 475.2 were shown in Fig. S9 (Fig. S9 was shown in Supplementary Material). In addition, Fig. 9 exhibited the oxidative degradation of TC in the 25% Co-MIL-53(Al)/PMS system. The TC molecules were attacked by radicals ($SO_4^{\cdot-}$ and $HO\cdot$) and non-radical ($^1O_2$) produced by the Co-MIL-53(Al)/PMS system, and transferred to other substances with lower molecular weight substances. These steps mainly involved dipolar cyclic addition towards double-bond [53], dislodging N—C bond and hydroxyl-substitution reaction [54], deamination, ring opening. As shown in Fig. 9, TC molecules were eventually oxidized to CO_2 and H_2O.

4. Conclusion

Based on the previously reported synthesis method [34], cobalt-doped MIL-53(Al) was prepared to activate PMS for TC degradation. The 25% Co-MIL-53(Al)/PMS system showed the best removal ability compared to the PMS alone and MIL-53(Al)/PMS systems, with the removal efficiency of TC and TOC reaching 94% and 51.5%. The system exhibited stability after four cycles and could resist the interference of solution pH and co-existing organic and inorganic ions and also showed high catalytic ability in actual water bodies (tap water, river water and pharmaceutical wastewater). The degradation of TC in Co-MIL-53(Al) activated PMS was mainly attributed to $SO_4^{\cdot-}$ radical and $^1O_2$ non-radical, and the active substances that played a role were consistent with those reported in other papers of studying degradation of organic pollutants by activating PMS [12,15,50]. The TC molecules were attacked by $SO_4^{\cdot-}$ radical and $^1O_2$ non-radical, then went through dipolar cyclic addition towards double-bond, dislodging N—C bond and hydroxyl-substitution reaction, deamination, ring opening and eventually turned into CO_2 and H_2O. The above results indicate that cobalt-doped MIL-53(Al) prepared by one-step solvent thermal method is a promising heterogeneous catalyst for activating PMS to degrade TC.

Declaration of Competing Interest

The authors declare that they have no known competing financial interests or personal relationships that could have appeared to influence the work reported in this paper.

Acknowledgement

The study was financially supported by the National Natural Science Foundation of China (51878258, 51521006 and 41807125).

Appendix A. Supplementary data

Supplementary data to this article can be found online at https://doi.org/10.1016/j.jcis.2020.07.100.

References

[1] M.Y. Jia, Z.H. Yang, H.Y. Xu, P.P. Song, W.P. Xiong, J. Cao, Y.R. Zhang, Y.P. Xiang, J. H. Hu, C.Y. Zhou, Y. Yang, W.J. Wang, Integrating N and F co-doped TiO_2 nanotubes with ZIF-8 as photoelectrode for enhanced photo-electrocatalytic degradation of sulfamethazine, Chem. Eng. J. 388 (2020) 124388.
[2] Z.H. Yang, J. Cao, Y.P. Chen, X. Li, W.P. Xiong, Y.Y. Zhou, C.Y. Zhou, R. Xu, Y.Y. Zhang, Mn-doped zirconium metal-organic framework as an effective adsorbent for removal of tetracycline and Cr(VI) from aqueous solution, Microporous Mesoporous Mater. 277 (2019) 277–285.
[3] Y. Bai, R. Xu, Q.P. Wang, Y.R. Zhang, Z.H. Yang, Sludge anaerobic digestion with high concentrations of tetracyclines and sulfonamides: Dynamics of microbial communities and change of antibiotic resistance genes, Bioresour. Technol. 276 (2019) 51–59.
[4] C.Q. Chen, L. Zheng, J.L. Zhou, H. Zhao, Persistence and risk of antibiotic residues and antibiotic resistance genes in major mariculture sites in Southeast China, Sci. Total Environ. 580 (2017) 1175–1184.
[5] R. Daghrir, P. Drogui, Tetracycline antibiotics in the environment: a review, Environ. Chem. Lett. 11 (2013) 209–227.
[6] Y. Zeng, N. Guo, H.Y. Li, Q.Y. Wang, X.J. Xu, Y. Yu, X.R. Han, H.W. Yu, Construction of flower-like MoS_2/Ag_2S/Ag Z-scheme photocatalysts with enhanced visible-light photocatalytic activity for water purification, Sci. Total Environ. 659 (2019) 20–32.
[7] Y.Y. Zhou, Y.Z. He, Y.Z. He, X.C. Liu, B. Xu, J.F. Yu, C.H. Dai, A.Q. Huang, Y. Pang, L. Luo, Analyses of tetracycline adsorption on alkali-acid modified magnetic biochar: Site energy distribution consideration, Sci. Total Environ. 650 (2019) 2260–2266.
[8] F. Ghanbari, M. Moradi, Application of peroxymonosulfate and its activation methods for degradation of environmental organic pollutants: Review, Chem. Eng. J. 310 (2017) 41–62.
[9] J. Cao, Z.H. Yang, W.P. Xiong, Y.Y. Zhou, Y. Wu, M.Y. Jia, S.W. Sun, C.Y. Zhou, Y.R. Zhang, R.H. Zhong, Peroxymonosulfate activation of magnetic Co nanoparticles relative to an N-doped porous carbon under confinement: Boosting stability and performance, Sep. Purif. Technol. 117237 (2020).
[10] J.Y. Cao, L.D. Lai, B. Lai, G. Yao, X. Chen, L.P. Song, Degradation of tetracycline by peroxymonosulfate activated with zero-valent iron: Performance, intermediates, toxicity and mechanism, Chem. Eng. J. 364 (2019) 45–56.
[11] X.G. Duan, C. Su, J. Miao, Y.J. Zhong, Z.P. Shao, S.B. Wang, H.Q. Sun, Insights into perovskite-catalyzed peroxymonosulfate activation: Maneuverable cobalt sites for promoted evolution of sulfate radicals, Appl. Catal. B 220 (2018) 626–634.
[12] K.-Y.-A. Lin, B.J. Chen, Magnetic carbon-supported cobalt derived from a Prussian blue analogue as a heterogeneous catalyst to activate peroxymonosulfate for efficient degradation of caffeine in water, J. Colloid Interface Sci. 486 (2017) 255–264.
[13] Q.Y. Song, Y.P. Feng, Z. Wang, G.G. Liu, W.Y. Lv, Degradation of triphenyl phosphate (TPhP) by $CoFe_2O_4$-activated peroxymonosulfate oxidation process: Kinetics, pathways, and mechanisms, Sci. Total Environ. 681 (2019) 331–338.
[14] H.Q. Sun, C. Kwan, A. Suvorova, H.M. Ang, M.O. Tadé, S.B. Wang, Catalytic oxidation of organic pollutants on pristine and surface nitrogen-modified carbon nanotubes with sulfate radicals, Appl. Catal. B 154–155 (2014) 134–141.
[15] J. Cao, S.W. Sun, X. Li, Z.H. Yang, W.P. Xiong, Y. Wu, M.Y. Jia, Y.Y. Zhou, C.Y. Zhou, Y.R. Zhang, Efficient charge transfer in aluminum-cobalt layered double hydroxide derived from Co-ZIF for enhanced catalytic degradation of tetracycline through peroxymonosulfate activation, Chem. Eng. J. 382 (2020) 122802.
[16] Y.F. Li, L.Y. Pan, Y.Q. Zhu, Y.Y. Yu, D.B. Wang, G.J. Yang, X.Z. Yuan, X.R. Liu, H.L. Li, J. Zhang, How does zero valent iron activating peroxydisulfate improve the dewatering of anaerobically digested sludge?, Water Res. 163 (2019) 114912.
[17] Y.R. Wang, W. Chu, Photo-assisted degradation of 2,4,5-trichlorophenoxyacetic acid by Fe(II)-catalyzed activation of Oxone process: The role of UV irradiation, reaction mechanism and mineralization, Appl. Catal. B 123–124 (2012) 151–161.
[18] Y.H. Guan, J. Ma, X.C. Li, J.Y. Fang, L.W. Chen, Influence of pH on the Formation of Sulfate and Hydroxyl Radicals in the UV/Peroxymonosulfate System, Environ. Sci. Technol. 45 (2011) 9308–9314.
[19] J. Liu, Q. Yang, D.B. Wang, X.M. Li, Y. Zhong, X. Li, Y.C. Deng, L.Q. Wang, K.X. Yi, G.M. Zeng, Enhanced dewaterability of waste activated sludge by Fe(II)-activated peroxymonosulfate oxidation, Bioresour. Technol. 206 (2016) 134–140.
[20] J.K. Du, J.G. Bao, Y. Liu, S.H. Kim, D.D. Dionysiou, Facile preparation of porous Mn/Fe_3O_4 cubes as peroxymonosulfate activating catalyst for effective bisphenol A degradation, Chem. Eng. J. 376 (2019) 119193.
[21] H.Z. Chi, X. He, J.Q. Zhang, D. Wang, X.D. Zhai, J. Ma, Hydroxylamine enhanced degradation of naproxen in Cu^{2+} activated peroxymonosulfate system at acidic condition: Efficiency, mechanisms and pathway, Chem. Eng. J. 361 (2019) 764–772.
[22] Y.Y. Ahn, H. Bae, H.I. Kim, S.H. Kim, J.H. Kim, S.G. Lee, J. Lee, Surface-loaded metal nanoparticles for peroxymonosulfate activation: Efficiency and mechanism reconnaissance, Appl. Catal. B 241 (2019) 561–569.
[23] L.H. Hou, X.M. Li, Q. Yang, F. Chen, S.N. Wang, Y.H. Ma, Y. Wu, X.F. Zhu, X.D. Huang, D.B. Wang, Heterogeneous activation of peroxymonosulfate using Mn-Fe layered double hydroxide: Performance and mechanism for organic pollutant degradation, Sci. Total Environ. 663 (2019) 453–464.
[24] Y.B. Ding, W.S. Nie, W.J. Li, Q. Chang, Co-doped $NaBiO_3$ nanosheets with surface confined Co species: High catalytic activation of peroxymonosulfate and ultra-low Co leaching, Chem. Eng. J. 356 (2019) 359–370.
[25] L.D. Lai, J.F. Yan, J. Li, B. Lai, Co/Al_2O_3-EPM as peroxymonosulfate activator for sulfamethoxazole removal: Performance, biotoxicity, degradation pathways and mechanism, Chem. Eng. J. 343 (2018) 676–688.
[26] H.Q. Luo, Y. Xie, J.Y. Niu, Y.X. Xiao, Y.L. Li, Y.B. Wang, Y.K. Zhang, T.H. Xie, Cobalt-doped biogenic manganese oxides for enhanced tetracycline degradation by activation of peroxymonosulfate, J. Chem. Technol. Biotechnol. 94 (2019) 752–760.

[27] T. Araya, M. Jia, J. Yang, P. Zhao, K. Cai, W.H. Ma, Y.P. Huang, Resin modified MIL-53(Fe) MOF for improvement of photocatalytic performance, Appl. Catal. B 203 (2017) 768–777.
[28] M.R. Azhar, P. Vijay, M.O. Tadé, H.Q. Sun, S.B. Wang, Submicron sized water-stable metal organic framework (bio-MOF-11) for catalytic degradation of pharmaceuticals and personal care products, Chemosphere 196 (2018) 105–114.
[29] H. Furukawa, K.E. Cordova, M. O'Keeffe, O.M. Yaghi, The chemistry and applications of metal-organic frameworks, Cheminform 341 (2013) 974.
[30] Q. Yang, Q. Xu, H.L. Jiang, Metal-organic frameworks meet metal nanoparticles: synergistic effect for enhanced catalysis, Chem. Soc. Rev. 46 (2017) 4774–4808.
[31] K. Zhang, D.D. Sun, C. Ma, G.L. Wang, X.L. Dong, X.X. Zhang, Activation of peroxymonosulfate by $CoFe_2O_4$ loaded on metal-organic framework for the degradation of organic dye, Chemosphere 241 (2020) 125021.
[32] N. Nagarjun, A. Dhakshinamoorthy, A Cu-Doped ZIF-8 metal organic framework as a heterogeneous solid catalyst for aerobic oxidation of benzylic hydrocarbons, New J. Chem. 43 (2019) 18702–18712.
[33] J. Cao, Z.H. Yang, W.P. Xiong, Y.Y. Zhou, Y.R. Peng, X. Li, C.Y. Zhou, R. Xu, Y.R. Zhang, One-step synthesis of Co-doped UiO-66 nanoparticle with enhanced removal efficiency of tetracycline: simultaneous adsorption and photocatalysis, Chem. Eng. J. 353 (2018) 126–137.
[34] Z.Q. Jia, M.C. Jiang, G.R. Wu, Amino-MIL-53(Al) Sandwich-Structure Membranes for Adsorption of p-Nitrophenol from Aqueous Solutions, Chem. Eng. J. 307 (2017) 283–290.
[35] L. Hu, W.F. Zhao, F. Zhen, Hydrophobic Pd nanocatalysts for one-pot and high-yield production of liquid furanic biofuels at low temperatures, Appl. Catal. B 215 (2017) 18–27.
[36] L.L. Liu, X.S. Tai, N.N. Zhang, Q.G. Meng, C.L. Xin, Supported Au/MIL-53(Al): a reusable green solid catalyst for the three-component coupling reaction of aldehyde, alkyne, and amine, React. Kinet. Mechan. Catal. 119 (2016) 335–348.
[37] C. Li, Z.H. Xiong, J.M. Zhang, C.S. Wu, The Strengthening Role of the Amino Group in Metal-Organic Framework MIL-53(Al) for Methylene Blue and Malachite Green Dye Adsorption, J. Chem. Eng. Data 60 (2015) 3414–3422.
[38] T. Loiseau, C. Serre, C. Huguenard, G. Fink, F. Taulelle, M. Henry, T. Bataille, G. Férey, A Rationale for the Large Breathing of the Porous Aluminum Terephthalate (MIL-53) Upon Hydration, Chemistry – A, European Journal 10 (2004) 1373–1382.
[39] Y.N. Hua, S. Wang, J. Xiao, C. Cui, C. Wang, Preparation and characterization of Fe_3O_4 /gallic acid/graphene oxide magnetic nanocomposites as highly efficient Fenton catalysts, RSC Adv. 7 (2017) 28979–28986.
[40] L. Tang, Y.N. Liu, J.J. Wang, G.M. Zeng, Y.C. Deng, H.R. Dong, H.P. Feng, J.J. Wang, B. Peng, Enhanced activation process of persulfate by mesoporous carbon for degradation of aqueous organic pollutants: Electron transfer mechanism, Appl. Catal. B 231 (2018) 1–10.
[41] X.G. Duan, C. Su, L. Zhou, H.Q. Sun, A. Suvorova, T. Odedairo, Z.H. Zhu, Z.P. Shao, S.B. Wang, Surface controlled generation of reactive radicals from persulfate by carbocatalysis on nanodiamonds, Appl. Catal. B 194 (2016) 7–15.
[42] L. Zhang, X.F. Zhao, C.G. Niu, N. Tang, H. Guo, X.J. Wen, C. Liang, G.M. Zeng, Enhanced activation of peroxymonosulfate by magnetic Co_3MnFeO_6 nanoparticles for removal of carbamazepine: Efficiency, synergetic mechanism and stability, Chem. Eng. J. 362 (2019) 851–864.
[43] G.D. Fang, D.D. Dionysiou, Y. Wang, S.R. Al-Abed, D.M. Zhou, Sulfate radical-based degradation of polychlorinated biphenyls: Effects of chloride ion and reaction kinetics, J. Hazard. Mater. 227–228 (2012) 394–401.
[44] C.Q. Tan, N.Y. Gao, D.F. Fu, J. Deng, L. Deng, Efficient degradation of paracetamol with nanoscaled magnetic $CoFe_2O_4$ and $MnFe_2O_4$ as a heterogeneous catalyst of peroxymonosulfate, Sep. Purif. Technol. 175 (2017) 47–57.
[45] W.D. Oh, Z.L. Dong, T.T. Lim, Generation of sulfate radical through heterogeneous catalysis for organic contaminants removal: Current development, challenges and prospects, Appl. Catal. B 194 (2016) 169–201.
[46] W.J. Ren, J.K. Gao, C. Lei, Y.B. Xie, Y.R. Cai, Q.Q. Ni, J.M. Yao, Recyclable metal-organic framework/cellulose aerogels for activating peroxymonosulfate to degrade organic pollutants, Chem. Eng. J. 349 (2018) 766–774.
[47] Q.X. Yang, X.F. Yang, Y. Yan, C. Sun, H.j. Wu, J. He, D.S. Wang, Heterogeneous activation of peroxymonosulfate by different ferromanganese oxides for tetracycline degradation: Structure dependence and catalytic mechanism, Chem. Eng. J. 348 (2018) 263–270.
[48] J. Li, J.L. Zhu, L.Z. Fang, Y.L. Nie, N. Tian, X.K. Tian, L.Q. Lu, Z.X. Zhou, C. Yang, Y. Li, Enhanced peroxymonosulfate activation by supported microporous carbon for degradation of tetracycline via non-radical mechanism, Sep. Purif. Technol. 240 (2020) 116617.
[49] C.H. Wang, J. Kim, M.J. Kim, H. Lim, M. Zhang, J. You, J.H. Yun, Y. Bando, J.S. Li, Y. Yamauchi, Nanoarchitectured metalorganic framework-derived hollow carbon nanofiber filters for advanced oxidation processes, J. Mater. Chem. A 7 (2019) 13743–13750.
[50] C.X. Li, J.E. Wu, W. Peng, Z.D. Fang, J. Liu, Peroxymonosulfate activation for efficient sulfamethoxazole degradation by Fe_3O_4/β-FeOOH nanocomposites: coexistence of radical and non-radical reactions, Chem. Eng. J. 356 (2019) 904–914.
[51] R.L. Yin, W.Q. Guo, H.Z. Wang, J.S. Du, X.J. Zhou, Q.L. Wu, H.S. Zheng, J.S. Chang, N.Q. Ren, Enhanced peroxymonosulfate activation for sulfamethazine degradation by ultrasound irradiation: Performances and mechanisms, Chem. Eng. J. 335 (2018) 145–153.
[52] C. Gong, F. Chen, Q. Yang, K. Luo, F.B. Yao, S.N. Wang, X.L. Wang, J.W. Wu, X.M. Li, D.B. Wang, Heterogeneous activation of peroxymonosulfate by Fe-Co layered doubled hydroxide for efficient catalytic degradation of Rhoadmine B, Chem. Eng. J. 321 (2017) 222–232.
[53] X.D. Zhu, Y.J. Wang, R.J. Sun, D.M. Zhou, Photocatalytic degradation of tetracycline in aqueous solution by nanosized TiO_2, Chemosphere 92 (2013) 925–932.
[54] M.H. Cao, P.F. Wang, Y.H. Ao, C. Wang, J. Hou, J. Qian, Visible light activated photocatalytic degradation of tetracycline by a magnetically separable composite photocatalyst: Graphene oxide/magnetite/cerium-doped titania, J. Colloid Interface Sci. 467 (2016) 129–139.